SUPPLEMENTARY INFORMATION

From One Building to Many: Transferability of A Deep Reinforcement Learning Agent For Optimizing Pollutant Exposure and Energy Consumption

Nishchaya Kumar Mishra[1], Sameer Patel[1, 2, 3, *]

[1]Department of Civil Engineering
[2]Department of Chemical Engineering
[3]Kiran C. Patel Centre of Sustainable Development
Indian Institute of Technology Gandhinagar
Palaj, Gandhinagar
Gujarat 382355, India

Submitted to
Environmental Science: Advances

[*]To whom correspondence be addressed: sameer.patel@iitgn.ac.in

Section S1. Training House Information and Layout

Table S1. House Parameters and HVAC & DASS Operating Conditions. Table adapted from Mishra et al. [1]

Volume (V)	250 m^3	Air Pressure	101253 Pa
Pressure Drop across DVS and HVAC fan	250 Pa	Set Temperature (T_{set})	25°C
Infiltration rate at 0.5 h^{-1}	9 µg/min	Conductivity of house (α) (single unit)	0.068 kJ s^{-1} C^{-1}
Variable flow rate through DASS (λ_{DASS})	0.5-10 h^{-1}	Air density	1.168 kg/m^3
Air change rate through HVAC (λ_{HVAC})	8 h^{-1}	EER of HVAC	3.10
Maximum Power consumption of HVAC	3 kW		

A comprehensive description of the field study design was presented by Farmer et al. [2] and more details about the test house, operating conditions, experimental design, instrumentation, and pollutant sources have been discussed previously [2–4]. Briefly, the three-bedroom test house has a floor area of ~111 m^2 and a volume of ~250 m^3. All measurements concerning this work were performed with all external doors and windows closed while a dedicated air supply system (DASS) maintained an outdoor-indoor AER of 0.5±0.1 h^{-1}. The installed heating, ventilation, and air conditioning (HVAC) system is a typical residential system for the conditioning of the recirculating air. The air handling unit (AHU) of the HVAC system operated continuously without a filter. The continuous AHU flow rate of 2000 m^3 h^{-1}, equivalent to 8 air changes per hour (ACH), minimized spatial gradients. During the field study, two kinds of experiments were performed: low-emission (LE) and high-emission (HE). LE activities were further bifurcated into two different categories: (1) LE1, where a real-life day was replicated by cooking three meals (breakfast, lunch, and dinner) and floor mopping, and (2) LE2, where one dish was cooked multiple times throughout the day at regular intervals [2]. HE activities included preparing a typical American Thanksgiving meal for about 14 persons. Particulate matter (PM) source strengths, infiltration rates, and deposition rates estimated using the measurements by Patel et al. [3,4] for nine different experimental days (four LE1s, two HEs, and three LE2s) have been used as input for this study. A comprehensive description of the field study design has been presented by Farmer et al. [2]. 4-532 nm particles were measured using two units of Scanning Mobility Particle Sizers (SMPS, TSI Inc.) [2–4].

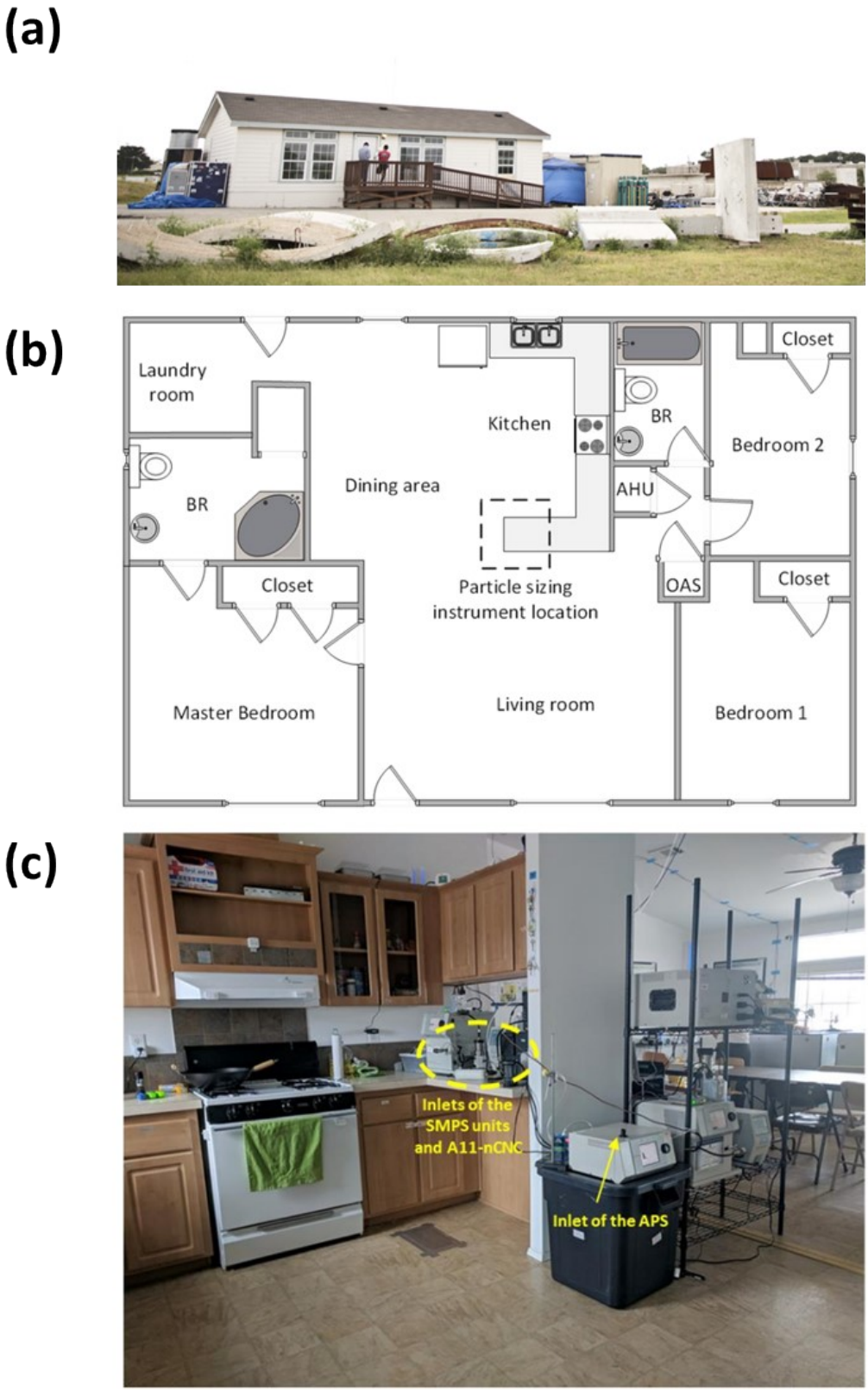

Figure S1. (a) The exterior view of the UTest House (adapted from Farmer et al. [2]), (b) floorplan of the house (adapted from Patel et al. [3]), and (c) interior view of the test house looking at the kitchen, living room areas, and the instruments (adapted from Patel et al. [3]). AHU: air handling unit, OAS: outdoor air supply, and BR: bathroom

Section S2. Monitored Parameters During the Field Study, Data Augmentation, Data Curation, and Digital Twin of the House for Reinforcement Learning Agent Training

During the field study, the test house was equipped with a range of monitors to measure or detect in real-time the energy consumption, temperature, size-resolved PM concentration, and RH at different locations. More details about these measurements are available in Farmer et al. [2]. Patel et al. [4] modeled various particle properties using size-resolved (4-500 nm) particle number size distribution measurements from two Scanning Mobility Particle Sizers (SMPS, TSI Inc., Shoreview, MN) collected at a 5-minute resolution. This study derives cumulative mass emission rates (ERs) from the size and time-resolved ERs reported by Patel et al. [3]. ERs derived for nine distinct cooking activities (four LE1s, two HEs, and three LE2s) have been used to train and test the deep reinforcement learning (DRL) agent. For training, ERs for six days (three LE1s, two LE2s, and one HE) have been used to create emission data for 20 days. Data augmentation techniques such as slice and shuffle, scaling, and permutation [5] have been applied to increase the density of the ERs for robust training of the DRL agent. The longitudinal ERs used for training the agent are presented in Figure S2, along with the curated outdoor Temperature, RH, and $PM_{2.5}$ concentration.

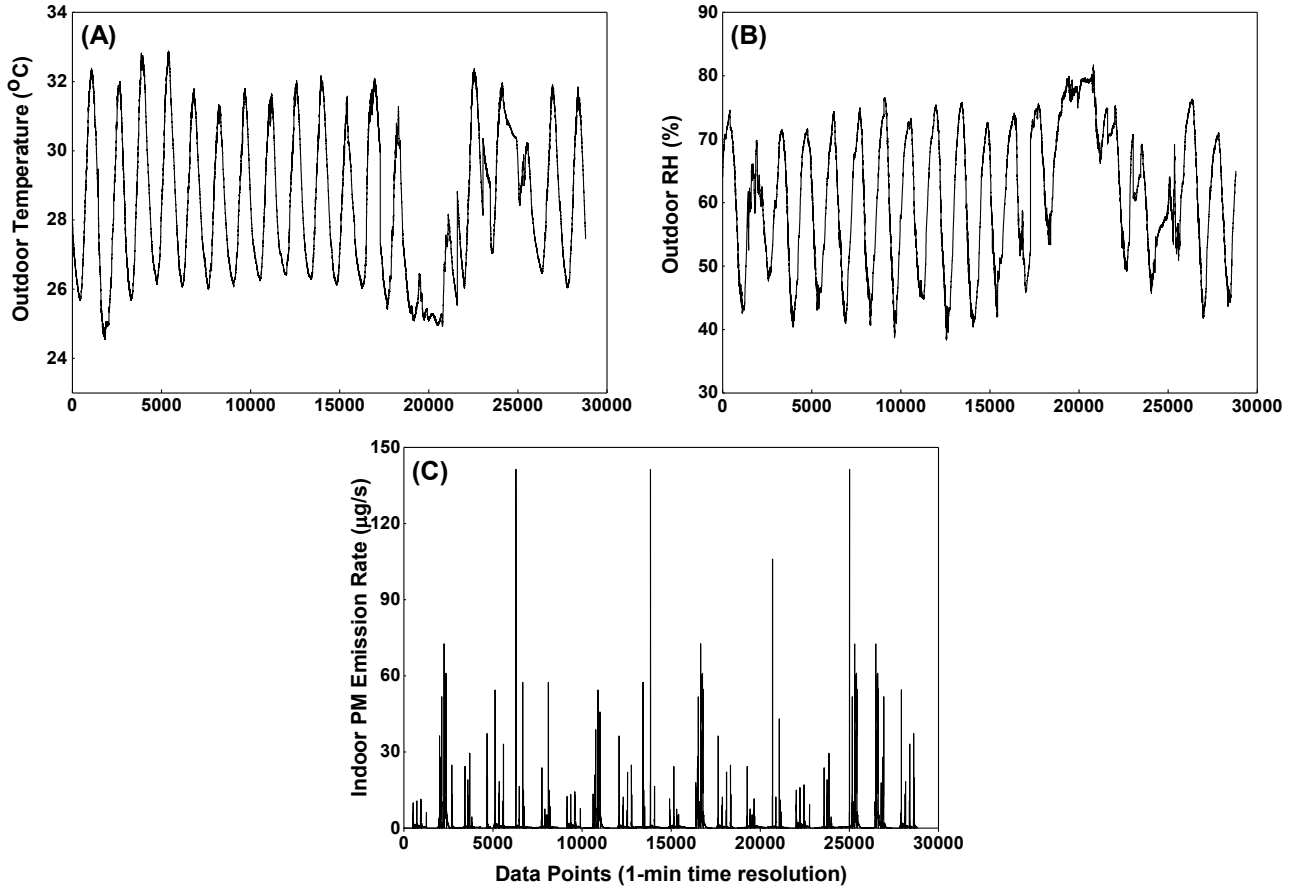

Figure S2. (A) Measured outdoor Temperature, (B) measured RH, and (C) estimated indoor PM emission rates for training the DRL agent at 1-min resolution. Figure adapted from Mishra et al. [1]

For offline training of the DRL agent, a digital twin of the test house that comprises indoor aerosol dynamics, operation of HVAC and DASS, and power consumption has been created. Fig. S3 presents a schematic of the test house with a DASS for outdoor air exchange and an HVAC system for air conditioning and indoor air recirculation. Eq. S1 presents a material balance model for indoor PM in a well-mixed volume [6].

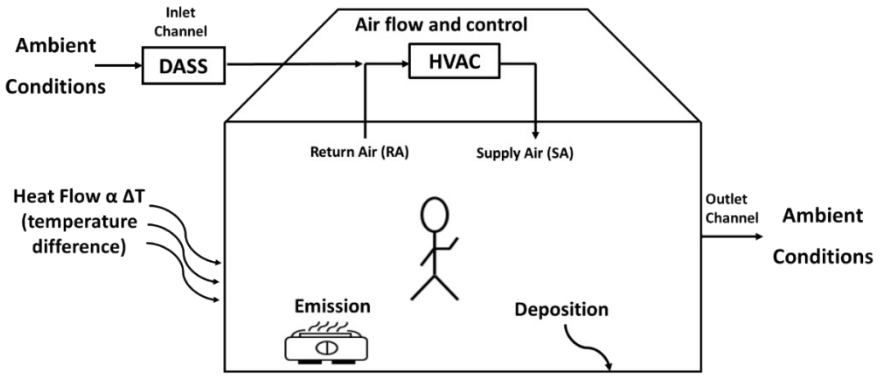

Figure S3. A schematic of the test house shows a dedicated air supply system (DASS) and a heating, ventilation, and air conditioning (HVAC) system.

$$\frac{dC_{in}}{dt} = \lambda_{DASS}\, p_{DASS}\, C_{out} - \lambda_{DASS}\, C_{in} + \frac{ER}{V} - \left(1 - p_{HVAC}\right) C_{in}\, \lambda_{HVAC} - DR\, C_{in}$$

Eq. S1

Where C_{out} is ambient PM concentration (μg/m^3), p_{DASS} is the PM penetration factor of the DASS, C_{in} is indoor PM concentration (μg/m^3), IR is the infiltration rate of outdoor PM (μg/min), λ_{DASS} is indoor-outdoor AER (min^{-1}), ER is the emission rate of PM from indoor sources (μg/min), V is the volume of the test house (m^3), p_{HVAC} is the PM penetration factor for the HVAC filter, λ_{HVAC} is recirculated air change rate (min^{-1}), and DR is PM surface deposition rate (min^{-1}). The input parameters, such as ERs and DR in Eq. (1), have been adopted from Mishra et al. [6].

An energy balance model is used to estimate the indoor air temperature and RH as a function of the outdoor air properties, HVAC operation, and heat exchange with the outdoor environment. The outdoor air (through DASS) was mixed with the return air of the HVAC system before the air conditioning unit (Fig. S3), which operated intermittently to ensure an indoor temperature of 25^{o}C. The net enthalpy change of the indoor air is expressed in Eq. S2 [7,8].

$$\frac{dh_{in}}{dt} = \left(\lambda_{DASS} + \lambda_{HVAC}\right)\left(h_{SA} - h_{in}\right) + \alpha\frac{T_{out} - T_{in}}{V\,\rho_{air}}$$

Eq. S2

where h_{in} and h_{SA} are the enthalpies of indoor air and supply air in kJ/kg, respectively; α (kW/^{o}C) is a measure of the thermal permeability of the house, and ρ_{air} is air density in kg/m^3. The first term represents the enthalpy change due to mixing the indoor air and supply air, and the second is the heat transfer due to the differences between outdoor and indoor temperatures. The discussion on α, its dependence on various factors, and the limitations of the model adopted in this work have been discussed by Mishra et al. [6]. This work focuses on a comparative analysis of different control strategies (DRL and DynOpt) with the benchmark conditions, which refer to personal exposure, energy consumption, and thermal comfort during the field study. The benchmark and the DynOpt proposed in the earlier study [6] have similar assumptions. Therefore, such assumptions should not affect the insights and results presented here. Other input parameters, such as outdoor air temperature and RH, were measured during the field study and used for simulations in this work. Further, Eq. S3 is applied to estimate water content changes in indoor air when mixing with outdoor air and supply air [9,10].

$$\frac{dw_{in}}{dt} = \left(\lambda_{DASS} + \lambda_{HVAC}\right)\left(w_{SA} - w_{in}\right)$$

Eq. S3

where w_{in} and w_{SA} are the water content of indoor air and the supply air in gm H_2O/kg air, respectively. The indoor air temperature is subsequently derived from the relationship between the thermodynamic properties of air presented in Eq. S4 [7]. More details about the HVAC operation, Eq. S4, and RH estimation are available in Section S3.

$$T = \frac{h - 2.5\,\omega}{1.01 + 0.00189\,\omega}$$

Eq. S4

where T is the Temperature in ^{o}C and ω is the specific humidity of indoor air in gm H_2O/kg dry air. The energy consumption of the air conditioning unit depends on the enthalpy change between mixed air and supply air. The enthalpies of mixed air (entering the HVAC system) and the supply air are estimated using Eq. S5 and Eq. S6, respectively [7].

$$h_{mixed} = \frac{\lambda_{DASS}\,h_{out} + \lambda_{HVAC}\,h_{in}}{\lambda_{DASS} + \lambda_{HVAC}}$$

Eq. S5

$$h_{SA} = T_{SA}\left(1.01 + 0.00189\,\omega_{SA}\right) + 2.5\,\omega_{SA}$$

Eq. S6

The total energy consumption *(E),* including DASS and the AHU unit, is estimated using Eq. S7.

$$E = \frac{\rho_{air}\,\lambda_{HVAC}\,V\left(h_{mixed} - h_{SA}\right)}{EER} + \frac{\Delta P_{HVAC}\;\lambda_{HVAC}\,V}{\eta_{HVAC}} + \frac{\Delta P_{DASS}\;\lambda_{DASS}\,V}{\eta_{DASS}}$$

Eq. S7

where ΔP_{HVAC} and ΔP_{DASS} are pressure drops in Pascal across the AHU and DASS, respectively, and η_{HVAC} and η_{DASS} are the AHU and DASS efficiencies. The pressure drops and efficiency values are adopted from Patel et al. [4].

Section S3: HVAC Operation and the Relationship Between Various Thermodynamic Properties of Air Streams

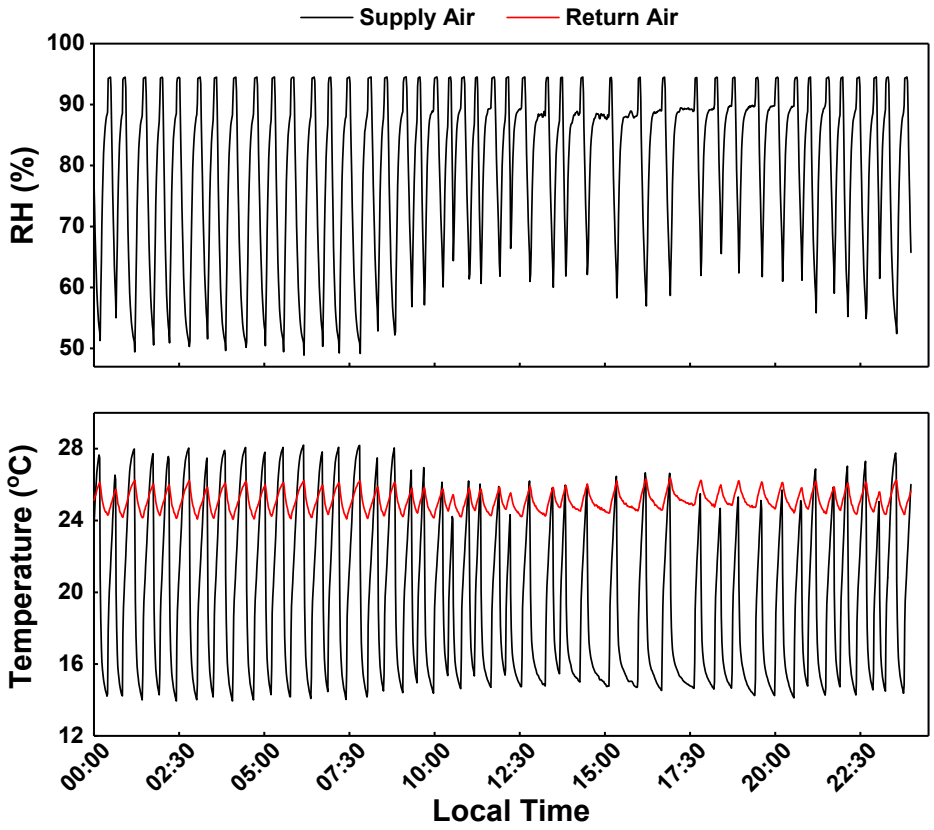

Figure S4. Temporal variations in relative humidity (RH) and temperature of return air and supply air for one of the experimental days during the field study. The figure is adapted from Mishra et al. [6]

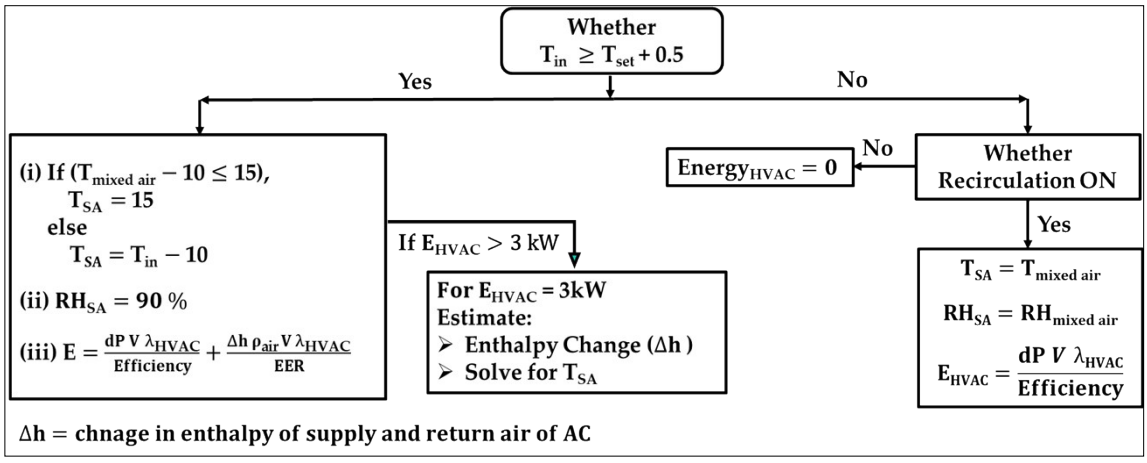

Figure S5. Flowchart illustrating the framework for the operation of the HVAC system in the test house. The terminology used in the flowchart is described in appropriate places. Figure adapted from Mishra et al. [6]

The psychrometric charts are used to estimate various thermodynamic properties of air. However, integrating psychrometric charts is computationally intensive, which can be addressed by the empirical relationships proposed in previous studies [11]. Empirical relationships utilized to estimate different air properties in this work are presented below. The saturation pressure is calculated using Eq. S8 [11].

$$P_{sat} = \frac{e^{\left(34.494 - \frac{4924.99}{T + 237.1}\right)}}{(T + 105)^{1.57}}$$

Eq. S8

where P_{sat} is saturation pressure in Pa, and T is Temperature in °C

Similarly, relations between vapor pressure, water content (w), saturation pressure (P_{sat}), and relative humidity (RH) are shown in Eq. S9 and Eq. S10 [7]. These relations are used to estimate the other properties if any two of them are known.

$$vapor\ pressure\ \frac{w\ P_{atm}}{621.9907}$$

Eq. S9

$$vapor\ pressure = RH\ \frac{P_{sat}}{100}$$

Eq. S10

where, *vapor pressure* is in Pascal, w is in gm H_2O/kg air, P_{atm} is the air pressure in Pascal, RH is relative humidity in %, and P_{sat} is saturation pressure in Pascal

The enthalpy of air (h) is governed by its Temperature (T) and specific humidity (ω), i.e., the mass of water per unit mass of dry air. The empirical relationship between the enthalpy of air, Temperature, and specific humidity is shown in Eq. S11.

$$h = T\ (1.01\ +\ 0.00189\omega)\ +\ 2.5\omega$$

Eq. S11

h is in kJ/kg, T is in °C, and ω is in gm H_2O / kg dry air

The specific humidity needed to estimate the enthalpy of air is estimated using Eq. S12.

$$\omega = \frac{621.9907\ vapour\ pressure}{P_{atm} -\ vapour\ pressure}$$

Eq. S12

where, *vapor pressure* and P_{atm} are in Pascal.

Section S4: Assessment of Parameters in the Cost Function

Mishra et al. [6] expressed the cost function as shown in Eq. S13, where the first component is energy consumption, and the second component is a measure of indoor PM exposure. They also discussed the effect of weightage factors, a-value, and threshold C_{max} on the trade-off between PM exposure and energy consumption. The study proposed that a dynamic set temperature of the air conditioning unit may reduce the energy penalty associated with maintaining thermal comfort while reducing pollutant exposure [6]. This section briefly discusses key findings from the previous study.

$$minimize$$
$$obj\ =\ W_1E +\ W_2(\max(0, C - C_{max}))^a$$

Eq. S13

The energy-exposure trade-off has been quantified at W_1/W_2 values ranging from 0.01 to 100, as demonstrated in Fig. S6. The normalized exposure reduction measured the extent of exposure reduction with a unit percentage increase in energy consumption. Similarly, the variations in exposure and energy

consumption for different values of a and C_{max} have also been discussed by Mishra et al. [6] for two experimental days, LE1_2 and HE1, and presented in Figure S7 and Figure S8.

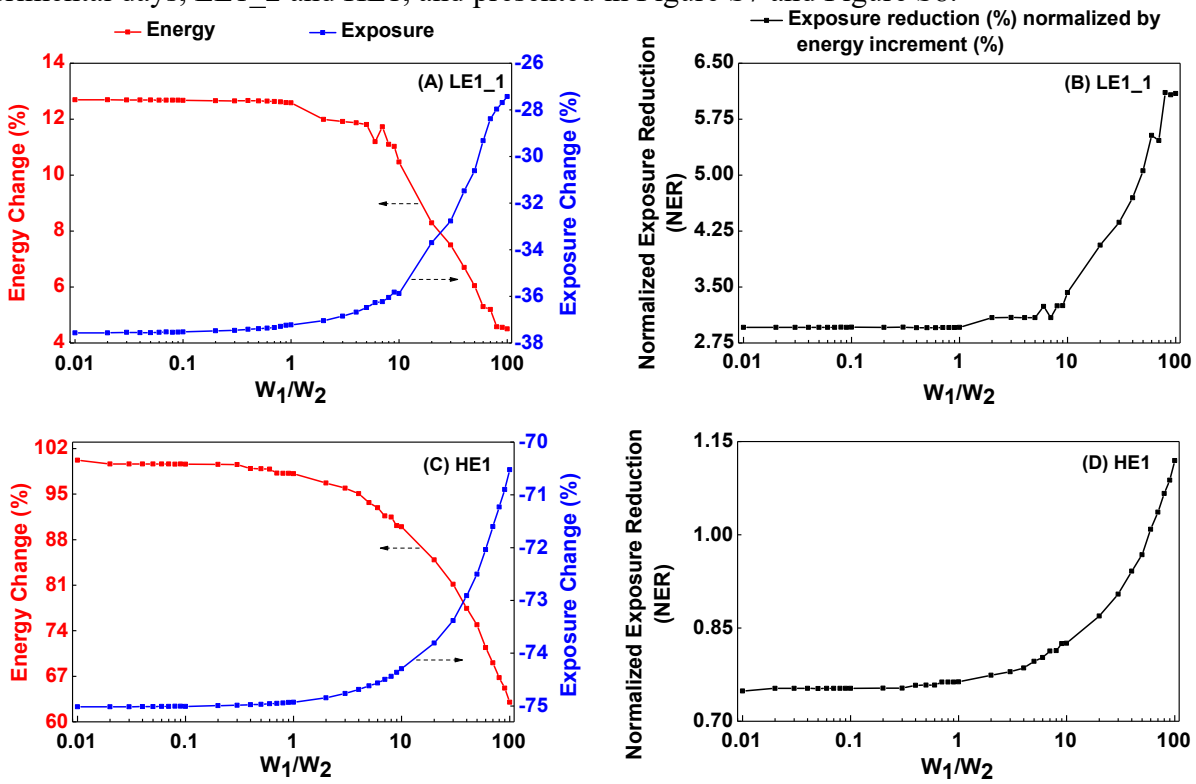

Figure S6. Sensitivity analysis of energy and exposure for LE1_2 and HE1 with distinct W_1/W_2 ratios where (A) and (C) are energy-exposure sensitivity, and (B) and (D) are variations of normalized exposure reduction (NER). (+) ve change means increment, and (-) ve change means reduction. Figure adapted from Mishra et al. [6]

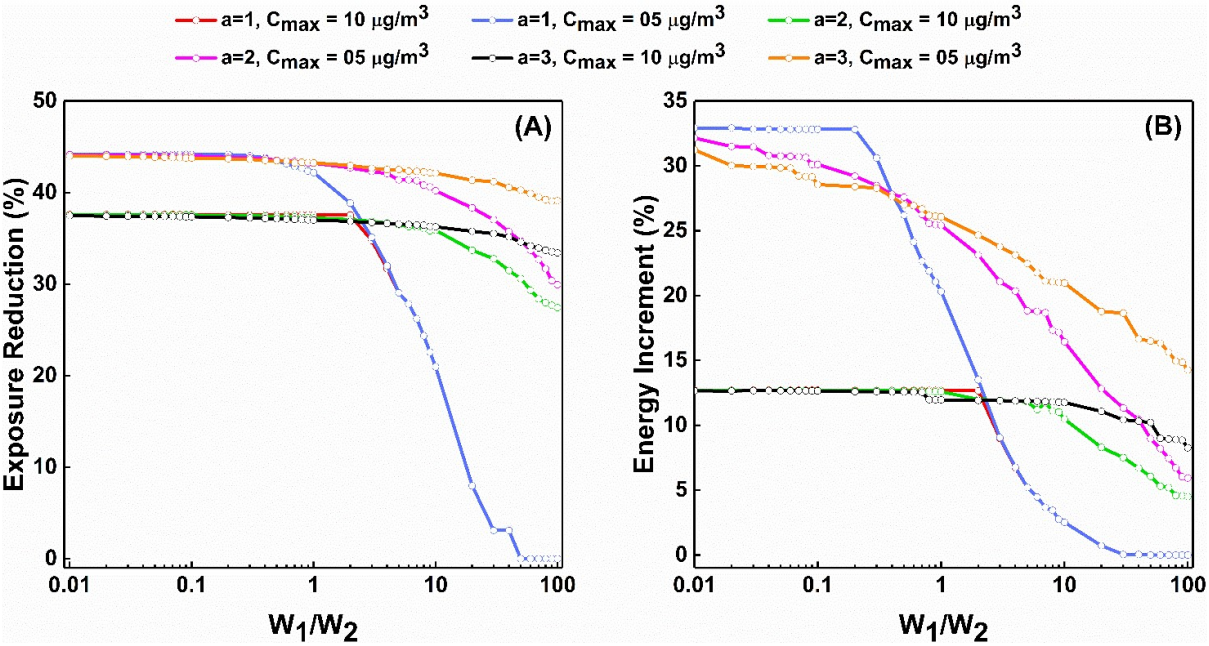

Figure S7. Sensitivity analysis of energy and exposure for LE1_2 experiment with distinct W_1/W_2 ratios (0.01 to 100) with a = 1, 2, 3, and C_{max} = 5 µg/m³ and 10 µg/m³ where % exposure reduction variations (A), and % energy consumption variations (B) are shown. Figure adapted from Mishra et al. [6]

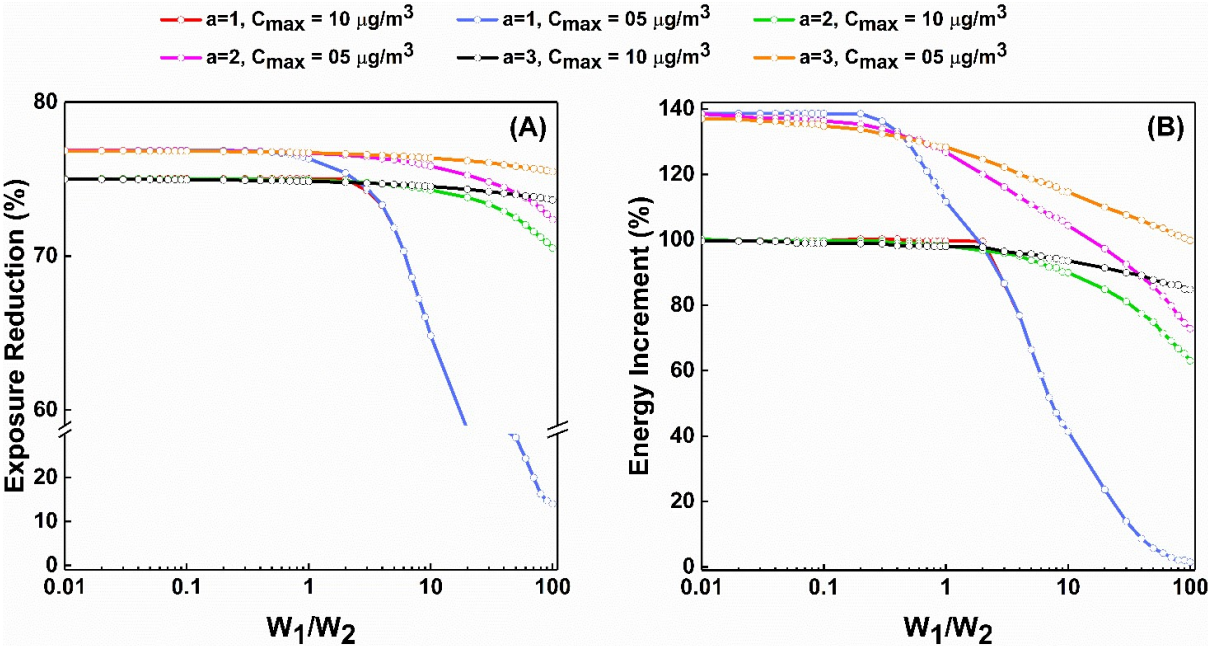

Figure S8. Sensitivity analysis of energy and exposure for HE1 experiment with distinct W_1/W_2 ratios (0.01 to 100) with a = 1, 2, 3, and C_{max} = 5 μg/m³ and 10 μg/m³ where % exposure reduction variations (A), and % energy consumption variations (B) are shown. Figure adapted from Mishra et al. [6]

References

[1] Mishra NK, Batra N, Patel S. Optimizing Pollutant Exposure, Energy Consumption, and Thermal Comfort in a House via Deep Reinforcement Learning Control. Journal of Building Engineering 2025:114074. https://doi.org/10.1016/J.JOBE.2025.114074.

[2] Farmer DK, Vance ME, Abbatt JPD, Abeleira A, Alves MR, Arata C, et al. Overview of HOMEChem: House Observations of Microbial and Environmental Chemistry. Environ Sci Process Impacts 2019;21:1280–300. https://doi.org/10.1039/C9EM00228F.

[3] Patel S, Sankhyan S, Boedicker EK, Decarlo PF, Farmer DK, Goldstein AH, et al. Indoor Particulate Matter during HOMEChem: Concentrations, Size Distributions, and Exposures. Environ Sci Technol 2020;54:7107–16. https://doi.org/10.1021/ACS.EST.0C00740/SUPPL_FILE/ES0C00740_LIVESLIDES.MP4.

[4] Patel S, Rim D, Sankhyan S, Novoselac A, Vance ME. Aerosol dynamics modeling of sub-500 nm particles during the HOMEChem study. Environ Sci Process Impacts 2021;23:1706–17. https://doi.org/10.1039/D1EM00259G.

[5] Iglesias G, Talavera E, González-Prieto Á, Mozo A, Gómez-Canaval S. Data Augmentation techniques in time series domain: a survey and taxonomy. Neural Comput Appl 2023;35:10123–45. https://doi.org/10.1007/S00521-023-08459-3/FIGURES/9.

[6] Mishra NK, Vance ME, Novoselac A, Patel S. Dynamic optimization of personal exposure and energy consumption while ensuring thermal comfort in a test house. Build Environ 2024;252:111265. https://doi.org/10.1016/J.BUILDENV.2024.111265.

[7] Engineering Toolbox. Mixing of Humid Air 2004. https://www.engineeringtoolbox.com/mixing-humid-air-d_694.html (accessed May 17, 2023).

[8] Afram A, Janabi-Sharifi F. Review of modeling methods for HVAC systems. Appl Therm Eng 2014;67:507–19. https://doi.org/10.1016/J.APPLTHERMALENG.2014.03.055.

[9] Dinçer I, Rosen M (Marc A). Exergy analysis of heating, refrigerating and air conditioning : methods and applications. n.d.

[10] Sala Lizarraga JMP, Picallo-Perez A. Exergy analysis and thermoeconomics of buildings : design and analysis for sustainable energy systems. n.d.

[11] Huang J. A Simple Accurate Formula for Calculating Saturation Vapor Pressure of Water and Ice. J Appl Meteorol Climatol 2018;57:1265–72. https://doi.org/10.1175/JAMC-D-17-0334.1.